Advancing flood warning procedures in ungauged basins with machine learning.

Zimeena Rasheed[1], Akshay Aravamudan[2], Ali Gorji Sefidmazgi[1], Georgios C. Anagnostopoulos[2], Efthymios I. Nikolopoulos[1*]

[1]Mechanical and Civil Engineering Department, Florida Institute of Technology, Melbourne, FL, USA.

[2]Computer Engineering and Sciences Department, Florida Institute of Technology, Melbourne, FL, USA.

*Corresponding author: Efthymios I. Nikolopoulos (enikolopoulos@fit.edu)

This manuscript has been submitted to the Journal of Hydrology (May 2021) but has not been peer reviewed yet.

It is submitted as an EarthArXiv preprint (May 2021).

Please feel free to contact the authors and share your feedback.

Abstract

Flood prediction across scales and more specifically in ungauged areas remains still a great challenge that limits the efficiency of flood risk mitigation strategies and disaster preparedness. Building upon the recent success of Machine Learning (ML) models on streamflow prediction, this work presents a prototype ML-based framework for flood warning and flood peak prediction. The fundamental elements of the proposed system consist of a) a LSTM model for classifying storm events to threat/no-threat given a threshold based on the 90th flow percentile and b) the flood peak prediction models. The selected ML-models for flood peak prediction are the Histogram based Gradient Boosting Regressor and the Random Forest. One of the strengths, and reason for selection, of these decision-tree models is their degree of interpretability. This is exploited in the study to help us spatially disentangle the role of both the static and dynamic drivers of flood peak response. Our analysis is presented for 18 distinct hydroclimatic regions across the contiguous US. Results reveal a significant regional dependence on both predictive performance and dominant flood predictors, which emphasize the variability in the complexity of a catchment's hydrologic behavior as well as its impact on modeling flood response. Evaluation of the drivers of flood peaks noted distinct dependencies among the dynamic and static predictors considered in our models for flood peaks of different severity. Specifically, low-moderate flood events showed a clear preponderance for the static catchment attributes over dynamic predictors like precipitation whereas precipitation was the dominant driver for the high severity flood peaks. The proposed flood peak prediction models were compared against a state-of-the-art LSTM model and were shown to consistently outperform in ungauged basins. Overall, the proposed system classified

storms correctly for >85% in all cases and exhibited a percent relative difference in flood peak estimates of <30% in most cases.

Keywords: Flood peak, prediction, machine learning, ungauged basins, flood warning

1. Introduction

To date, floods are the most recurring and devastating natural hazard affecting the contiguous United States (CONUS) posing significant risk to lives and livelihoods (Dougherty and Rasmussen 2019; Knight 2010; Perry 2000). Flood impacts within CONUS alone are associated with a significant toll on human life, and annual incurred costs of 6.2 billion USD for damages over the past decade (NCEI 2020). These are facts which enunciate the need to accurately predict flood events everywhere.

Streamflow, primarily in heavily and growing urbanized regions across CONUS, has been increasing; a trend noted for the last 50 years (Lins and Slack 2005). In addition, studies investigating the impacts of current and future climate extremes (Lins and Slack 2005; Milly et al. 2002; Sharma et al. 2018) indicate that the U.S. population is becoming alarmingly vulnerable to flood-associated risks (Naz et al. 2016; Wing et al. 2018). These trends are particular not only to CONUS but have been observed in other parts of the world, including Europe (Jarosińska and Pierzga 2017; Teuling et al. 2019), Central Asia (Gulakhmadov et al. 2020) and South America (Lara et al. 2017). Under various growth scenarios for future climate as prescribed by global climate models, and, despite local- and regional-scale complexities, this continual, upward intensification of median and high flows remains a consistent find in these studies.

The factors that lead to increase in peak flow are many. Arguably, precipitation is the dominant driver controlling peak flow response (Prein et al. 2017; Seneviratne et al. 2012; Slater and Villarini 2017) and there is virtually unanimous acknowledgement of current and future precipitation patterns intensifying. Exceptions to this trend exist (Ivancic and Shaw 2015; Westra et al. 2013) due to other atmospheric variables like temperature (Wasko and Sharma 2017) or potential evapotranspiration that may precede the impact of precipitation on peak flow response (Mallakpour and Villarini 2015). The argument regarding these exceptions continues that the other variables attributable to modulating extreme flood response (Hall et al. 2014; Merz et al. 2012) include regional and catchment-specific hydrogeomorphic parameters, water management schemes (National Research Council et al. 2007), soil and hydraulic parameters, as well as land-cover changes (Ahn et al. 2014; Kim and Kim 2020; Tomer and Schilling 2009), to name a few. In unique cases, we may see a specific factor controlling streamflow response, but the interaction among any of the above drivers is what makes the prediction of flood peaks (i.e. very high streamflow) a complex process (Hrachowitz et al. 2013; Saghafian et al. 2014; Todini 2007). Thus, we first need to understand these static and dynamic drivers and the specific role they play in peak flow response.

The ability to accurately predict streamflow across spatial scales has been an ongoing topic of research for several decades (Kratzert et al. 2018; Mosavi et al. 2018; Razavi Tara and Coulibaly Paulin 2013; Remesan and Mathew 2014; Slater and Villarini 2017). Indeed, accounting for the complexity and nonlinear interactions of land surface properties with dynamic forcing (precipitation, temperature) and state variables (soil moisture) to be able to accurately predict flood response still remains a challenging task.

Traditional approaches to simulating streamflow or peak discharge have been centered around the development of empirical as well as physics-based distributed hydrologic models (Ivanov et al. 2004; Kim et al. 2019; Lin et al. 2018; Razavi Tara and Coulibaly Paulin 2013; Todini 2007 among many others). The capability of accounting for spatial variability within a catchment and extensively informing on its hydrologic system are clear advantages of these approaches (Costabile and Macchione 2015). In return, they require extensive computational resources, and high-resolution spatial data related to catchment attributes and initial boundary conditions (Samaniego et al. 2010). For these reasons, distributed models are shied away from for large-sample studies and applications. With the growing concern of flood hazards increasing not only in severity but also in frequency and large areas still being ungauged, which poses a great limitation on parameterization of physics-based models, the hydrologic community has started investigating alternative models that has the potential to efficiently predict peak flows especially for ungauged catchments. Such investigations led to the implementation of data-driven models utilizing machine-learning (ML) algorithms (Kratzert et al. 2019b; Mosavi et al. 2018; Remesan and Mathew 2014; Xiang et al. 2020).

The potential for ML-based approaches towards simulating streamflow among other hydrologic applications (Elshorbagy et al. 2010; Kasiviswanathan et al. 2016; Schoppa et al. 2020) has been noted for well over a decade now, but broader exploration was attempted only recently. Over the last few years, the availability of large-sample, high-resolution, observed and simulated hydrometeorological datasets have enabled the analysis of various flood generation processes at the catchment scale along with their drivers. ML-based models alleviate the intensive computational resources required of physics-based distributed models whilst maintaining the necessary design (and processing) complexity, and predictive strength desired (Mosavi et al. 2018; Todini 2007). However, accurate peak flow prediction remains challenging. For example, the LSTM-based neural network of (Kratzert et al. 2018), requires vast meteorological, historic data as input and is able to capture exceptionally well the signals of low to moderate level flows. However, accurate predictions of very high flow events remain challenging. The devastating aftermath of missing these events has been outlined above which underlines the pressing need for improved prediction of such events for individual catchments.

The overarching goal of this study is to develop ML-based models aimed at accurately predicting peak flows. In contrast to the recent works published on the topic of ML-based streamflow prediction where the target contains the prediction of the entire spectrum of streamflow values, we develop a framework that is based on events (rainfall-to-runoff) and focuses solely on the prediction of flood peaks (i.e. single max flow value per rainfall event). Our framework also includes an ML-based classifier that separates storm events into flood and no-flood inducing. Integration of those elements is proposed as an alternative framework for flood forecasting in ungauged basins. En-route to this goal, we also seek to understand the dominant drivers of flood response and their dependence on hydroclimatic regime and flood severity.

The remainder of this paper is organized as follows. The study area and key steps to pre-process the data for peak flow analysis are described in Section 2. The methodological framework which explores two approaches to developing models capable of predicting peak flows in ungauged basins is detailed in Section 3. Section 4 presents the results of our ML-based models for different hydroclimatic zones and flow severities and discusses inferences drawn related to drivers of flood response, including the potential thereafter for advancing early-warning systems on floods. Future directions for building on this research and the main conclusions follow in Section 5.

2. Study Area and Data

This study utilized the CONUS-wide dataset *Catchment Attributes and MEteorology for Large-sample Studies* (CAMELS), which contains data for approximately 670 catchments (Addor et al.

2017; Newman et al. 2015). Hydrometeorological forcing includes precipitation, temperature and vapor pressure, to name a few, whilst the 30+ static catchment attributes are further subdivided into hydrological, climatic, vegetative, soil and topographical features. CAMELS provides hydrometeorological data based on the Daymet-derived, gridded estimates of daily weather parameters (Thornton et al. 2012) for these catchments from 1980 to 2014. Analysis was performed at a regional scale by clustering the catchments according to the regional watershed boundaries established by the United States Geological Services (USGS). Across CONUS, there are 18 distinct hydroclimatic regions designated by their two-digit Hydrologic Unit Code (HUC-02). The spread of the 670 catchments within each region is shown in Figure 1. The drainage areas of these catchments range from 3 km^2 to 25,524 km^2 with an average of 589 km^2.

2.1. Pre-processing

2.1.1. Identification of Peak Flows

Given that the focus of our investigation is on the prediction of peak flows, the very first step required was to process the available streamflow time series and identify the peak flow events. The peak events were defined as flows above a threshold established at the 90th quantile streamflow value for any given catchment (see Figure 2). Peak flows above this threshold allowed us to capture and focus our analysis on the highest flow conditions relevant to flood events. The time-series for all selected catchments were processed with flood peaks extracted across 43 full water years for 598 catchments. The temporal record of streamflow observations for the remaining catchments was shorter if the gauge station was established later than 1980 or ceased operation before 2014. For these catchments, the meteorological forcing time-series was trimmed to match the shortened streamflow record. By this procedure, we were able to retain data pertaining to the 670 catchments identified in Figure 1, such that we have all regions represented.

From the flow values exceeding the defined threshold, the selection of peak flows was further restrained using the following criteria: first, to ensure independence among flood events considered in any catchment's streamflow record, peak events selected should be separated by a minimum time interval. The calculation of this time separation (θ) followed the work of (Hu et al., 2020) and is a function of the area of the catchment.

$\theta\ > 5\ days + 2.59 \times log\ (A)$ - Eqn. (1)

where A is the catchment area measured in km^2.

Second, any selected peak corresponding to a triggering storm event that exceeded 14 days in duration was excluded from the dataset; refer to Section 2.1.2 for more details. Our flood peak database numbered approximately 67,000 entries at the end of processing the time-series with an average of 100 peak flows identified per catchment. Table 1 details the distribution of flood peaks in each of the 18 regions. To enable spatial analyses, each flood peak was normalized by the area of the respective catchment.

2.1.2. Attributing Triggering Storm

All storms for any given catchment were first separated by user-defined thresholds: (1) the minimum inter-storm period considered was one day, which corresponded also to the minimum available temporal resolution since we were dealing with daily time series (2) precipitation must record at least 1 mm/day to be considered a part of a storm. Having identified all unique storms across the length of the precipitation series, we then matched the streamflow time series with the precipitation storm series taking note of start and end times of all storms. As shown in Figure 2, we then looked for the storm that preceded this peak; more specifically, a storm whose start preceded the beginning of the rising limb of the peak. Some storms continued past the peak we were interested in, but, this extra precipitation does not contribute to the triggering precipitation that caused the flood peak and in these instances we considered precipitation only up to the time of the peak. It is worth mentioning that both precipitation and streamflow were available at daily timesteps. Selected characteristics of the triggering precipitation identified for each peak event corresponded to the maximum, mean and total event precipitation. Based on the days attributed as part of the triggering storm, other meteorological-forcing data such as the daily maximum temperature was also used by taking averages over the respective period.

2.1.3. Accounting for antecedent wetness

The last dynamic variable considered and reported in our peak-event delineated datasets (or flood peak database), is a measure of antecedent wetness condition (AWC). Information on the AWC of the soil is one factor that modulates runoff generation and, hence, affects peak flow. While its importance is expected to vary for different catchments, its impact on peak flow generation has been clearly demonstrated in several past studies (Nikolopoulos et al. 2011; Pathiraja et al. 2012; Saadi et al. 2020). The antecedent precipitation index (API) was the chosen proxy for representing the recent moisture state of the catchment right before the start of the triggering storm. It's definition, seen in Eqn. (2), follows the work presented by (Kohler and Linsley 1951) and is the basis for the "retained rainfall" model by Singh (1988).

$API = \sum_{j=0}^{i} P_{t-j} \ k^{j}$ - Eqn. (2)

where i = total number of antecedent days; j = lag or antecedent time of interest (days), P_t= the precipitation recorded on day t and k = decay constant which ranges from 0.8-0.98 (Viessman and Lewis 1996) with 0.9 used as the estimate for this study.

We also considered the use of the normalized antecedent precipitation index (NAPI) which factors in the mean precipitation thereby allowing for sounder regional comparisons (Ali et al. 2010; Heggen 2001). However, preliminary findings (not shown here) revealed that API was a stronger predictor of flood peak than NAPI and thus we decided to employ API as the proxy for AWC of the catchments. The API was constructed across a 30-day time frame prior to and ending the day just before the start of the triggering storm for any identified peak in the dataset. Applicable temporal lengths for expressing API typically include 7, 14 or 30 days with meteorological and hydroclimatic variables influencing this choice from one catchment to the next, not discounting seasonal variances. We investigated the aforementioned API durations and observed that a 30-day period was nearly optimum for use across the 18 different regions.

Following the pre-processing phase of the dynamic variables, the static attributes corresponding to the respective catchments were incorporated into the dataset. This final combination formed the flood peak database, which this study then used.

3. Methodology

3.1. Analysis Framework

One of the main goals of this work was the development of regional models for predicting flood peaks based on hydrometeorological data and catchment attributes. The ML-based models were used to predict normalized, to catchment area, peak flows. There were two experiments designed to evaluate the peak prediction abilities of the models in ungauged catchments. The design of Experiments 1 and 2 (Figure 3) differed in the data available as input for the prediction models. The training and validation datasets prepared for Experiment 1 ensured that events from each of the 670 catchments were contained in each dataset. In simpler terms, Experiment 1 prepared the datasets for a "gauged catchment" scenario i.e. ML models were used to predict flood peaks for catchments that were included in the training data. Experiment 2 instead had unique catchments in each of the datasets prepared emulating an "ungauged catchment" scenario. As such, the models' performance in this experiment were validated for ungauged catchments since they were not present during the training phase. With this approach, we were able to check for catchment dependencies affecting model prediction capability. Experiment 1 had the additional role as a benchmark for comparing the peak prediction performance of the regional models in the ungauged scenario, Experiment 2.

To evaluate the overall added value of the developed models, their performance was compared against a state-of-the-art approach (see Section 3.4 for details). Accuracy in prediction at catchment scale has been posited for models aggregating hydrologically homogeneous basins (Kratzert et al. 2019b; Razavi Tara and Coulibaly Paulin 2013). This similarity in behavior at regional scale can be learned by carefully designed models to then predict at the local scale. Our study area emphasized 18 distinct hydroclimatic regions (Figure 1) corresponding to 18 models for every chosen ML-model.

Notably the training datasets contained 60 percent of the flood peak database and of the 40 percent for validation, 10 percent was withheld as the final test set. The remaining 30 percent was specifically used for selecting good model hyper-parameter values. Finally, the resulting models' generalization performance was assessed on the test set, which are presented in this study.

3.2. Selection of Predictor Variables

Following the discussion above on hydrometeorological drivers of peak flow response, we utilized three derivations of precipitation and one of temperature as dynamic inputs for our models. These were narrowed to: (i) the maximum precipitation, (ii) the mean precipitation, (iii) the mean daily maximum temperature recorded during the period of each triggering storm, and (iv) API, as a measure of antecedent wetness condition (see Section 2.1.3). Other dynamic inputs during exploratory analysis had considered variables related to minimum temperature, vapor pressure and accumulated triggering precipitation. These, however, did not markedly improve predictions and, hence, were omitted from further consideration. A similar procedure as taken with the time series was tried for the static attributes, where we noted very specific instances of improvement, with a higher dimensioned dataset (i.e. larger quantity of features used by models). Albeit, on average, improvement was negligible across the 18 regional models. As such, over the negligible decreased performance, we prioritized the reduced complexity of the models, by using only 3 static attributes. The static attributes selected considered the forested fraction, the soil porosity and the mean potential evapotranspiration record for each catchment. Needless to say, these are variables that studies (Hall et al. 2014; Merz et al. 2012) have alluded to as key catchment-specific drivers of peak flow response and allows the hydrologist to draw understanding of hydrologic behavior based on model performance. To evaluate the role of these predictors within each region, a measure of predictor importance was assessed during modeling, the details of which are provided in section 3.3 below.

3.3. Development of Predictive Models

An important motivation when utilizing ML-based approaches for regression is their generalization ability and their interpretability. While decision tree regressors are highly interpretable compared to their deep-learning counterparts, we required our models to be accurate while, at the same time, less prone to overfitting. Ensemble models are used to improve weak base learners, such as decision trees (typically, stumps thereof), by aggregating their predictions in a variety of different ways. As such, we decided to adopt two ensemble methods: Histogram based Gradient Boosting Regressor (Ke et al. 2017) and Random Forest (Breiman 2001; Ho 1995). Rule extraction from such ensemble models is much more difficult (NP-hard) than it is for decision trees, although there have been attempts to approximate these rules (Cui et al. 2015). However, these models do allow for the computation of permutation feature importance (Breiman 2001), which helped us compare their relative importance, as they pertained to flood response. Physics-based models are by construction "interpretable", an ability mostly lost when transitioning to ML-based models such as LSTM-based neural networks. Our selected ML models, however, by virtue of these feature importance, were able to retain some attribution as interpretable models. Permutation feature importance measures were obtained by permuting individual feature values among the training samples and evaluating the error induced as a result. Feature value permutations that produced higher errors under a trained model were deemed important. Such feedback offered the additional advantage of allowing us to improve our understanding about the drivers of peak flow events and their relative significance across different hydroclimatic regions. As described in

Section 3.2, we used 7 variables, all of which were continuous variables. The objective function being minimized was the Mean Square Error (MSE) and as a result, it was used as a metric to compare the performance of models in each region.

In addition to the models that considered all available peak flows in the dataset (All-Flows), we developed models that segmented the flood peak dataset into low-moderate (LM-Flows) and high flows (H-Flows). The threshold for discriminating between these two types of flows was set to the 75th percentile recorded among the normalized flood peaks in each region. We hypothesized that although the events in our flood peak database captured the highest 10 percent of flows in any given catchment, the role of the predictors we later selected as input for our models varied even within this limited range.

The RF technique is a bagging method that involves bootstrapping the data, training several base learners (decision trees) and aggregating the results from these base learners to extract predictions. This ensemble, tree-based method has seen previous applications in this field of study. In particular, RF models in the field of hydrology have proven useful in flood risk analysis and susceptibility mapping (Zhao et al. 2018), rainfall forecasting (Taksande and Mohod 2015) with performance close to that of Support Vector Machines (Yu et al. 2017; Mosavi et al. 2018), and, in recent studies, seen as advantageous in large-scale flood discharge simulations (Schoppa et al. 2020). These models are less prone to overfitting since an increasing number of base learners leads to a converging generalization error (see Theorem 1.2 in Breiman 2001). As opposed to the standard splitting criteria for decision trees (i.e. CART based), these base learners determine splits using Generalized, Unbiased Interaction and Detection Estimation (GUIDE, see Loh 2002). More specifically, the selected method chooses a split that minimizes the p-value of a chi-square test of pairwise independence among all possible splits. Following tuning of the size of the ensemble, we observed that using 150 trees for RF minimized the validation MSE for each region.

The HGBR method is a Gradient Boosting Machine (Friedman 2001) that aims to learn the underlying function as a linear combination of regression trees, also referred to as base learners. This is approached in a stagewise fashion that involves adjusting the previously learned function using a greedy step (gradient based line search method) towards the data-based estimate of the function. Gradient boosting is one such model that aims at learning a linear combination of base learners, optimizing each successive learner using the gradient of the loss function with respect to the current function estimate, which in our case was MSE. Every new learner attempts to improve upon the shortcomings of its predecessors. Several applications in the hydrological domain have reaped the benefits of gradient boosting; Extreme Gradient Boosting has been used to assess flood susceptibility (Mirzaei et al. 2021) and groundwater spring potential (Naghibi et al. 2020). Gradient Boosting was also used in conjunction with Gaussian Mixture Models for streamflow forecasting (Ni et al. 2020). We have adopted a more scalable version of the Gradient Boosting algorithm, namely the HGBR model, inspired by the LightGBM model (Ke et al. 2017). More specifically, we used the algorithm implemented in scikit-learn (Pedregosa et al. 2011), which is a ML library for the Python programming language. The splitting criterion for each node in the tree follows the standard method which aims to choose the split that minimizes the residual sum of squares. Hyper-parameters such as number of estimators, maximum number of leaves per learner, the ℓ^2 regularization parameter for the learned weights, and the learning rate were fine-tuned for each HGBR model per region and were selected to minimize the validation MSE.

3.4. LSTM-based Approach

Current state of the art in the ML-based prediction of continuous streamflow has utilized Long-Short Term Memory (LSTM) cells in the design of neural networks (Kratzert et al. 2018; Kratzert et al. 2019a; Xiang et al. 2020) to the task at hand. Although our study is focused on predicting the peak streamflow during storm events, these prior LSTM-based works that predict continuous streamflow serve to provide benchmark performances that we can compare with. Additionally, to the best of our knowledge, there is a lack of literature that directly predicts the peaks, as a result, we resort to models that have an overarching objective of time series prediction that could perform well in this setting. LSTMs are Recurrent Neural Networks architectures capable of learning time series with long-term dependencies (Hochreiter and Schmidhuber 1997). Prior such models seemed to perform well in the time points related to low and moderate level flows. However, for the time instances that are identified as flood peaks (i.e. extreme values) performance decreases and oftentimes associates with underestimation of the high flows as has been verified in our experiments; refer to Section 4.1 for more details.

The methodology for streamflow prediction in (Kratzert et al. 2018) was adopted for this study and, as such, we used the same LSTM architecture provided by the authors of Kratzert et al. (2018) as well as the spatial application of the models to CONUS. Notably, Kratzert et al. (2018) also used the CAMELS dataset. For each of the 18 hydroclimatic regions, the hydrometeorological time series (including precipitation, minimum and maximum temperatures, solar radiation and vapor pressure) of all catchments in the training dataset were stacked, preprocessed, then fed to the LSTM model to be trained. Having trained the model, the LSTM forecasts the validation data for each catchment. As per Kratzert et al. (2018), the sequence length of the input to the LSTM layer is 365 (days). Kratzert et al. (2018) used a two-layer LSTM network, with each layer having 20 LSTM cells. Between the layers, a dropout layer with a rate of 0.1 was added as a measure to prevent overfitting (Srivastava et al., 2014).The batch size was 2048 and each LSTM model was trained for 20 epochs. The LSTM-based approach used the 'RMSprop' optimizer with a learning rate of 0.001. All facets of the code provided by the authors of Kratzert et al. (2018) remained intact with the exception of the data it was fed and the hyper-parameters.

3.4. A proposed framework for flood warning systems

As a final integrative step of this work, we proposed a framework that combines a flood detector with the flood peak predictive models developed for flood warning applications. We provide a methodology on aggregating and systematically processing relevant meteorological data to detect storms likely to deliver peak flows. For the demonstration of the "flood detector", we maintained the definition of a flood peak as one above the 90th quantile streamflow in a given catchment. Spatial analyses bearing on the idea behind using 18 distinct hydroclimatic regions was maintained for the detector. Meteorological forcing constitutes the only data used as input for the flood detector. Precipitation (mm/day), minimum and maximum temperatures (°C) and solar radiation (W/m^2) were the specific, dynamic predictors input as time series. This selection was narrowed from available time series including vapor pressure, antecedent precipitation index (a derivative of precipitation) as well as static catchment attributes. These final variable choices, despite their importance to the detector's task, are all easily accessible via remote-sensing datasets today, be it as historic, recent past, or near future (numerical weather prediction forecasts) timeseries. The dependence of the flood detector on these variables was thus justified hydrologically, as they greatly impact streamflow generation, and operationally, as they can be conveniently sourced at reasonable temporal and spatial resolutions from remote-sensing systems and atmospheric models. Output from this flood detector was in binary form: "No flood (no peak expected)" or "Flood (peak expected)". In the first response case, the system continued to monitor the incoming meteorological data inputs and was ready to predict for the next timestep. If the latter, the follow-up was to employ a peak-prediction model (detailed in foregoing sections) to then quantitatively estimate the peak flow expected.

The detector incorporates LSTM cells to process multiple meteorological time series. For a given window size, these meteorological, time-series, variables are each passed through an LSTM layer consisting of 20 cells. The outputs of these LSTM layers are then concatenated and propagated through a series of dense layers to produce the output label. The flood detector model used: the 'RMSprop' optimizer with a learning rate of 0.001, batch size of 2000 trained for 30 epochs and a binary cross entropy loss function. The loss function was weighted to balance the two classes since there was a prevalence of No-Flood events in the dataset for each catchment. With time series as input, the window size indicates the temporal span of data required by the detector to produce predictions. Receiver Operating Characteristic (ROC) curves are useful for assessing detection performance. Specifically, performance was gauged by comparing the estimated hit rate (proportion of flood events successfully detected, also referred to as true positive rate) given different window sizes for a fixed 20% estimated false alarm rate (proportion of events that were erroneously labeled as flood events).

4. Results & Discussion

This section is subdivided into the following four parts. First, we showcase and narrate the results of our peak prediction models compared to the LSTM-based approach for both Experiments 1 and 2. Second, we evaluate the models' performance for different flood severity levels. The third section disentangles the results of the peak flow models to explain the role of the hydrometeorological and catchment-specific predictors employed. The fourth subsection presents the framework for incorporating the flood detector, such as the one we developed as an early-warning tool.

4.1. Regional performance of prediction models

4.1.1. Experiment 1

A comparison of the HGBR, RF, and the LSTM-based peak prediction models for Experiment 1, is shown in Figure 4. Regional model performances are indicated for the All-Flows scenario and measured using the Root Mean Squared Error (RMSE) metric. To expound on the differences between the three models, we employed the Wilcoxon Signed Rank (WSR) test, with the null hypothesis being that the models perform indistinguishably (i.e., RMSE samples for all models are drawn from the same distribution). Non-parametric, WSR tests were selected after conducting Shapiro-Wilks tests where the results rejected the null hypothesis that the data distribution was normal, at 5% significance. For any given region, 10 equally spaced quantile RMSE scores (at 10^{th}, 20^{th}, …, 90^{th} and 100^{th} quantiles) to represent all the events in each region are computed and paired-WSR tests were carried out at 95% confidence level. The tests revealed statistically significant differences between the performances of the LSTM and HGBR models for 16 regions. Of these, the LSTM has the most difficulty along the Pacific Northwest and Southwest coasts which see most instances of flood peaks concentrated during the winter and early-spring seasons; a consequence of the atmospheric rivers that traverse the regions during these periods. The null hypothesis was not rejected for Regions 13 and 15, indicating similar performance. At the same confidence level, the LSTM and RF models performed significantly dissimilar for all regions except Regions 10, 13 and 15. These U.S. West-Central regions have fewer flood events with a heavy skew towards flash floods brought about by warmer convective atmospheric conditions during the summer. These flood peaks are among the lowest recorded across CONUS and may explain the similar performance between the LSTM and the peak prediction models since the LSTM better simulates low-moderate peaks.

The regional Wilcoxon signed rank tests revealed that there were no significant differences between the performance of the HGBR and RF for 9 regions (p-value > 0.05). The 9 other regions, primarily located in the US-East, negated this trend and showed that there were significant differences in the performance of the two models for these regions.

4.1.2. Experiment 2

Experiment 2 was designed specifically to represent an ungauged scenario where the catchments in the training and validation datasets were unique. However, regional representation of catchments was ensured (see section 3.1 for details). We therefore fulfilled the criteria of being able to predict in ungauged catchments, with the median RMSE performance per region shown in Figure 5. Similar to Experiment 1, Wilcoxon Signed Rank tests were carried out for the regional models comparing the LSTM and HGBR, the LSTM and RF and the HGBR and RF. At 95% confidence level, the tests revealed significant differences in performance for most regions in the test scenarios against the LSTM. Results for Regions 4, 9, 10, 12 and 15 in the LSTM and HGBR comparison, failed to reject the null hypothesis and, hence means that the models perform similarly. Results for Regions 4, 9, 10, 12, 15 and 16 in the LSTM and RF comparison, failed to reject the null hypothesis. We noted similar trends across the regions as highlighted in Experiment 1. However, comparing the HGBR and RF models, the Wilcoxon signed rank tests indicated that there were significant differences between the performance of the two models for 12 of the 18 modeled regions. The 6 regions that RF and HGBR statistically performed similarly in are regions 3, 4, 8, 11, 14 and 18.

A multiple comparison test applying the Holm-Bonferroni method (Holm 1979), which controls family wise error rate, was performed for each region at 5% significance level. Resultantly, the HGBR model was simultaneously better than the LSTM-based and RF models in all regions, for both experiments.

From a pragmatic perspective, a comparison of the LSTM model and peak prediction models between Experiments 1 and 2 is illustrated in Figure 6. Here, the percent relative difference (PRD) was used as the measure to compare the average observed peak flows and the predicted peak flows for each region. For the purpose of assessment, we considered the performance acceptable, if the PRD calculated for each region was ±30%. The HGBR and RF for Experiment 1 (see Figure 6) had PRDs within this ±30% threshold for all regions except for those along the Southwest Central Regions (10, 11 and 12). Models for the three outlier regions had a propensity to overestimate the flood peaks whilst the LSTM for all regions consistently underestimated the flood peaks. With the exception of Region 17, this underestimation exceeded the -30% PRD threshold.

For the ungauged scenario, Experiment 2 (see Figure 6), the HGBR and RF models also had acceptable PRD ranges for most regions. As opposed to the greater number of regions overestimating in Experiment 1, there was a mixed trend of over- and under-predicting across the regions for the HGBR and RF models for Experiment 2. We noted instances of underestimation for this experiment especially for the California region; -55% and -40% for the HGBR and RF models, respectively. The LSTM once again underpredicted the flood peaks for all regions except Regions 9 and 13. Overall, the problematic regions in both experiments considering both RMSE and PRD metrics, were the West coast, the Southern and Northern Central Regions and the Great Plains. The West coast with its Mediterranean-like climate, parts of the Southern and Northern Central regions which identify with drier climates and have one of the lowest annual precipitation totals across CONUS, and the Great Plains whose steep terrain and snowmelt during warmer periods, all impact the hydrologic signatures of the catchments within, and could potentially explain the performance of the models for these regions. Section 4.3 below offers more on understanding the predictors.

4.2. Evaluation of model performance across peak flow quantiles

The preceding discussion looked at performance for models considering all events in the respective datasets (All-Flows scenario). Now that we have established the predictive abilities of our peak-flow models, we will turn our attention to addressing the results of mainly the HGBR and RF models considering the flood severity classes, namely: LM-Flows and H-Flows.

In addition to the PRD plots shown in Figure 6, a quantile-quantile comparison is included in Figure 7 specific to the HGBR and RF models. Figure 7a for the HGBR model showed better agreement in predicted peak-flow quantiles compared to the RF model (Figure 7b). For both models, and for both experiments, we noted a tendency towards underestimation; a trend pronounced for the H-Flows scenario. The same was true for the All-flows scenario, but for the low-moderate flood severity, the RF distinctly overestimated. HGBR for LM-Flows had the closest agreement between the observed and predicted peak flows with averaged absolute relative difference values of 9.7% and 22.0% for Experiments 1 and 2, respectively.

Figure 8 provides regional PRD comparisons for LM-Flows and H-Flows for the two peak prediction models. Aside from the LM-Flows scenario of Experiment 1, the HGBR did not have a defined trend of under- or over-predicting. Conversely, the RF mostly overestimated low-moderate flood peaks and underestimated for the high flood severity. Evidently, HGBR is the better model for performing consistently across flood severities and further discussion will focus on the results of this model. For the ungauged experiment, the HGBR seemingly has difficulty for Regions 13, 4 and 16, the latter two especially for LM-Flows.

4.3. Understanding predictors

Notwithstanding the relative importance assigned to predictors as a product of using rule-based models, we only aimed to evaluate the role they play in flood response from one region to another and across differing flow severities. Figure 9 presents the relative importance of the predictors segmented by static and dynamic predictors for both LM-Flows (a) and H-Flows (b). Attention is focused on the selected HGBR model from the foregoing sections on performance evaluation.

4.3.1. Dynamic Predictors

With reference to Figure 9, for H-Flows, the dynamic predictors held greater importance at influencing peak prediction compared to the static catchment attributes. The opposite was true for LM-Flows.

Maximum and Mean Precipitation: The relative weights of triggering precipitation were clearly higher for H-Flows than LM-Flows, but for both severity levels, the maximum triggering precipitation having high feature importance implied a strong causal influence on flood peaks. Analyses of the intensity of the precipitation events as a ratio of the maximum precipitation to the total triggering precipitation of the regions indicated that, on average, the US Northeastern, Southeastern, North Central and Upper Colorado regions, had a greater number of H-Flows that were triggered by short duration, intensity-dominated storm events, than LM-Flows. Knowing that flood-inducing precipitation and their sources across CONUS, are regionally-defined, these identified precipitation patterns coincide with, for example, the recorded higher occurrences of flash type floods in the southeastern region (Dobur 2006), brought about by short-duration, high intensity air-thunderstorms; a consequence of the moisture passages from the Gulf of Mexico (Hirschboeck 1991). The presence of tropical storms and cyclone-related, flood-inducing, precipitation events that the southeastern US region is susceptible to especially during the warmer, late spring and early summer seasons may also justify this trend. In addition to convective storms mainly occurring in the late summer, early fall seasons, the Northeastern regions (Berghuijs et al. 2016), are vulnerable to flood-inducing precipitation resulting from snowmelt, or extra tropical cyclones and their associated fronts (vicinity of the Atlantic Ocean) influenced by warmer temperatures. The mountainous terrains at (1) the junction of the Northeastern and Southeastern regions and (2) along the Intermountain-West regions (notably Upper Colorado), are also susceptible to local flash floods resulting from similar convective storms enhanced by orographic lifting. The U.S. North Central regions with drier climates and low soil moisture retention capabilities, record the lowest magnitude of peak flows overall, with flash-type floods (classed as H-Flows) being the result of majority, short convective precipitation events in the region (Berghuijs et al. 2016; Hirschboeck 1991). Conversely, H-Flows in other regions whilst being triggered by higher magnitude, total precipitation, these storm events persisted for a longer duration with one example being the Great Basin. Here, floods with higher rise times occur in the steep, glacial terrain (Saharia et al. 2017) given the influence of snowmelt. The reduced importance of precipitation for LM-Flows point instead to the other drivers (see remaining discussion) that better support the precipitation-to-peak flow relationship.

Mean Maximum-Temperature: Two general regions placed exception to the trend of precipitation as the controlling predictor: the Northeastern and some parts of the Intermountain West regions. H-Flows in the energy-limited catchments of the U.S. Northeast are more influenced by temperature. Indeed, the distinct, four-season, climate of the U.S. Northeast has been changing over time with the increasing oceanic and atmospheric temperatures, the declining snow and ice density, the rising sea levels and strain on the ecosystem and hydrologic systems brought about by heavy urbanization of the region (Assessment 2018; Pan et al. 2004). As for the Intermountain West regions, temperature shares a similar magnitude of importance as precipitation for improving peak flow predictions. These regions are more water-limited but increasing daily minimum temperatures and increased early-summer rainfall, which mitigated daily maximum temperatures from rising, translated to higher flood peaks recorded (Kunkel et al. 2013; Pryor 2013).

Antecedent Precipitation Index: On average, the importance of API was weighted higher for LM-Flows. Generally, this class of flood severity is not driven by high intensity-short duration storms as is most often the case for H-Flows, where the sheer magnitude of runoff generated by the current storm is not affected by preceding precipitation. Unexpectedly, for H-Flows particularly within the Great Basins (#16), the inclusion of API mapped to better peak flow predictions. This finding may be rationalized by the influence of snowmelt in the region which increases in the warmer seasons of the year and coincides with the time that most flood peaks are observed; high flood peaks but with slow rise time, i.e., not intensity-dominated flows. For LM-Flows however, the current wetness condition of the catchment as a result of preceding storm events greatly affects the flood response in the catchment and the models particularly for the Southern Central regions viewed API as an important dynamic predictor. As an interface between the extreme precipitation regimes of the Eastern and Western CONUS regions, the hydrologic signature in these regions is influenced accordingly by pre-event, precipitation excess, wetness brought about by thunderstorms common in the region during the monsoon periods.

4.3.2. Static Predictors

Forest Fraction: For LM- and H-Flows, the relative importance of forest fraction was minimal for the regions along the Eastern and Western coasts. This trend is best rationalized by placing into perspective the changes in land use over the last few decades (Alig et al. 2003). The Northeastern US is deemed a heavily-urbanized region therefore we see little to no influence from forest fraction on flood peak prediction. Instead, the South and Southwest regions including the West Intermountain areas which have seen growing populations, especially within the last two decades, have recorded decreased fractions in forest cover as the rural to urban shift is made (Alig et al.

2004; Kunkel et al. 2013). It is within these recently changing regions that the variability of forest cover among catchments heightened and, thus played an important role in flood peak prediction, especially for Low-Moderate flows.

Soil Porosity: The physics behind soil hydraulic characteristics impacting streamflow response is complex. Of the catchment attributes related to soil from the CAMELS dataset, soil porosity aided better predictions overall. Relative importance was higher among the LM-Flows with relatively higher impact in the Northern Central, Northern Great Plains and the Intermountain-West regions. Interestingly, the total precipitation in these regions was among the lowest of the 18 regions in this study. A plausible explanation for the importance of this feature to flood response may be attributed to the presence of wetlands in the areas which lie within the steep glacial moraine uplands (Verry and Kolka 2003). Seepage from these saturated bodies of water regulated in part by the soil hydraulic features like soil porosity of the surrounding areas eventually feed to channels causing the higher peak flows recorded (Dahl 2014; Sucik and Marks 2015). An additional explanation may be offered when looking at the weighted importance of this attribute in conjunction with mean PET. For those regions, which have a drier climate given elevated temperatures, surface infiltration rates are higher with increased (dried) pore space.

Mean PET: LM-Flows in the U.S. West were more responsive to PET than the U.S. East (Figure 9a). Upon closer observation, the Intermountain West and Pacific regions were the most affected and duly so given their arid-steppe and Mediterranean like climates, respectively. The summers for both are especially hot leading to water-limited catchments (i.e. with higher PET values). As for higher flood severities (Figure 9b) the trend in PET was scattered across the regions but the models for the Lower Colorado and Pacific regions remained dependent on the mean PET for improved peak flow predictions. In the Northeast region, we saw an unexpected emphasis on the mean PET. With annual precipitation in excess of evapotranspiration, catchments in the Northeastern regions are traditionally categorized as energy-limited. Recent analyses have shown however that opposite to temperature, precipitation controls evapotranspiration (Vadeboncoeur et al. 2018) with summer precipitation having the highest correlation with evapotranspiration (than summer temperature). Moreover, the interplay between precipitation and evapotranspiration modulates antecedent wetness and can therefore have an important impact on flood response in humid catchments (Nikolopoulos et al. 2011).

4.4. Flood Detector

The duration/length of the time series (or time "window") required for the detection of flood inducing storms, was obtained experimentally by conducting analyses of accumulated timesteps (3 to 60 days) within each region to best determine its length. From ROC curves, performance was gauged by comparing the hit rate given different window sizes for a 20% false alarm rate. The flood detector provided optimal results across the 18 regions with a window size of 30 days, the results of which are presented in Figure 10(a). Notably, with a window size of 30 days, performance from the detector eventually reported the inclusion of API as negligible. This is understandable as the construction of this index for the study was based on a 30-day duration. Precipitation made available to the detector as a time series inherently accounts for antecedent moisture condition with a 30-day window size. Acknowledging that the actual duration of a flood inducing storm is at the order of one to few days (much less than the optimal 30-day window), emphasizes clearly the importance of antecedent conditions on the classification of the storms.

Figure 10(b) shows the corresponding area under the ROC curves (AUC) for the 18 regions presented in Figure 10(a). The hit rate (or sensitivity) is the detector's ability to correctly identify a flood peak event. With the exception of the Lower Colorado Region (#15), all regions were associated with a hit rate close to or above 80%. Accounting for the detector's ability to accurately identify "Flood" events, all regions recorded AUC scores of 85% and higher.

In addition to dynamic variables, static catchment attributes were tried as inputs. Following analyses, the impact of catchment attributes on the binary classification of flood inducing storms was not significant. Wide variability was expected as the region under study changed, but, given the above discussion on understanding the predictors of flood peaks, a sound basis for further exploring and developing this input arm of the detector exists.

Figure 11 provides an example of the operational flow for the proposed flood warning system. The example is based on a selected catchment from the test-dataset (ID: 12013500) located along the Willapa River near Willapa, Region 17. This framework asks two main questions: (1) at a time, t, do we expect a flood, and (2) if we are to expect a flood, what is the predicted magnitude of the peak? Following the discussion on the duration (number of timesteps) of the input required by the detector, we first identified the 30 days of precipitation, minimum and maximum temperatures and solar radiation, before time, t. The HGBR issued a prediction if the detector warned of an expected flood as was the case for the sampled event in Figure 11a from March 3 through 12, 2014. After a peak prediction was made, the loop was repeated for the next timestep of interest. For comparison, the observed streamflow is plotted along with the relevant predicted peak flows. The threshold distinguishing flood peaks is plotted at the 90th quantile streamflow for the catchment.

From observation, false positives issued by the detector are usually within vicinity of the 90th quantile threshold. As seen in Figure 11b, this is often the case for timesteps just preceding a major flood event (March 28, 2012) or on the recession limb of the flood hydrograph as flow level drops just below the threshold (April 5-7, 2012). This is surmised as an artifact of regional detector modeling where the 90^{th} quantile streamflow rates of catchments within a region are similar but not the same, thus, a range of uncertainty is present for each catchment within any given region.

Note that as long as the flood inducing storm remained close to forecasted time, t, the detector identified potential flood conditions (even when actual flood was in recession). Equivalently, the HGBR model kept providing peak flow predictions that were close in magnitude. As a reminder, this framework was developed to provide peak flow prediction whenever a flood was imminent and was not intended to predict the shape of the flood hydrograph. As such, the system can be used to provide expected max flood conditions during the entire period of the detected “flood” event. The duration of such an event can be derived from the flood detector.

5. Conclusions and Future Directions

A ML-based framework that addresses the detection of flood inducing storms and the prediction of flood peak magnitudes was developed and presented. Model training and validation were completed for 18 hydroclimatic regions across CONUS. It was demonstrated that ML-models, such as RF and HGBR, are suitable for predicting flood peaks at ungauged basins using a relatively small number of inputs. Specifically, derivatives of precipitation and temperature time series together with catchment attributes such as soil porosity, PET and forest fraction provided enough information to achieve flood peak predictions with less than 30% PRD in most regions across

CONUS. HGBR performed overall better than RF and both of them performed better than a state-of-art LSTM that was used for comparison. To a certain degree this is to be expected considering that RF and HGBR were developed solely for flood peak prediction while the LSTM was originally developed for predicting the entire flow spectrum. This fact therefore does not point necessarily to the best model but simply highlights that if having a skillful model for flood prediction is the objective, then it is preferable to develop predictive models only for flood events to avoid “stretching” them to accurately predict parts of the flow timeseries that may not be of importance. For the LSTM, it was shown that due to the latter, predictions for flood peaks were generally underestimated.

The relative simplicity of rule-based models such as RF and HGBR combined with their level of interpretability make them an attractive solution for developing predictive models in hydrology. Through analysis of the relative feature importance, it was shown that the factors influencing the generation of floods exhibit a strong regional dependence. Whilst precipitation-derived variables such as the maximum precipitation triggering a flood peak was found to control flood response significantly in most regions, catchment-specific attributes considering land cover (forest fraction), soil hydraulic features (soil porosity) and potential evapotranspiration also impact and improve the prediction of flood peaks. Notably, the impact of these highlighted drivers varied in response to the flood severity classes with catchment-specific attributes showing a higher degree of importance in the prediction of Low-Moderate flows than for High flows where instead precipitation dominated flood response. The dimension of seasonality was not considered, but previous research posits the ability to increase streamflow prediction. The inclusion of this dimension could potentially help to explain the residual behavior of the models in some regions such as those along the Northwest coast and upper-Northern regions of CONUS where precipitation regimes are unique.

Machine learning-based algorithms hold much potential for advancing flood predictions in ungauged catchments and therefore inform decisions on mitigation strategies for flood hazard. Our attempts at proactively dealing with the rise in extreme natural hazards have been focused on implementing and improving early-warning systems. In this work we propose a prototype flood warning system that combines a flood detector and the flood magnitude predictor. The detector (based on LSTM) is able to monitor meteorological conditions and issue warnings in case of an imminent flood, which subsequently trigger the peak prediction model (HGBR) that predicts the magnitude of the expected flood peak. Such a framework combined with remote sensing and numerical weather predictions can offer a potential solution for flood warning applications in areas where in situ observations are sparse or inexistent. Results from this work demonstrated that in all areas examined such a system would achieve a hit rate of greater than 85% for 20% false detections and while this recommends that there is definitely room for improvement, at the same time demonstrates arguably a lot of promise.

Moving forward, there are several steps that can be taken to further advance ML-based flood prediction and the development of warning procedures. First of all, integration of higher spatial and temporal variability of features considered is one important step towards advancing model development. So far, this and many other studies have used daily forcing data and catchment averaged values, while we know that dynamics of sub daily precipitation as well as its spatial distribution over a catchment affect flood response. Therefore, incorporating such information should be included in subsequent developments. Lastly, the transferability of the models produced in this and other works based on CAMELS dataset, should be evaluated globally by other similar datasets that have been recently developed (Alvarez-Garreton et al. 2018; Coxon et al. 2020).

Acknowledgements

The authors would like to thank Frederic Kratzert for sharing (via direct correspondence with Ali Gorji Sefidmazgi) the LSTM code used in Kratzert et al. 2018. Rasheed and Nikolopoulos were supported by National Science Foundation (grant #1934712).

References

Addor, N., Newman, A. J., Mizukami, N., & Clark, M. P. (2017). The CAMELS data set: catchment attributes and meteorology for large-sample studies. *Hydrology and Earth System Sciences*, *21*(10), 5293–5313. https://doi.org/10.5194/hess-21-5293-2017

Ahn, J., Cho, W., Kim, T., Shin, H., & Heo, J.-H. (2014). Flood Frequency Analysis for the Annual Peak Flows Simulated by an Event-Based Rainfall-Runoff Model in an Urban Drainage Basin. *WATER*, *6*(12), 3841–3863. https://doi.org/10.3390/w6123841

Ali, S., Ghosh, N. C., & Singh, R. (2010). Rainfall–runoff simulation using a normalized antecedent precipitation index. *Hydrological Sciences Journal*, *55*(2), 266–274. https://doi.org/10.1080/02626660903546175

Alig, R. J., Kline, J. D., & Lichtenstein, M. (2004). Urbanization on the US landscape: looking ahead in the 21st century. *Landscape and Urban Planning*, *69*(2), 219–234. https://doi.org/10.1016/j.landurbplan.2003.07.004

Alig, R. J., Plantinga, A. J., Ahn, S., & Kline, J. D. (2003). *Land use changes involving forestry in the United States: 1952 to 1997, with projections to 2050*. https://doi.org/10.2737/pnw-gtr-587

Alvarez-Garreton, C., Mendoza, P. A., Boisier, J. P., Addor, N., Galleguillos, M., Zambrano-Bigiarini, M., Lara, A., Puelma, C., Cortes, G., Garreaud, R., McPhee, J., & Ayala, A. (2018). The CAMELS-CL dataset: catchment attributes and meteorology for large sample studies – Chile dataset. Hydrology and Earth System Sciences, 22(11), 5817–5846. https://doi.org/10.5194/hess-22-5817-2018

Assessment, C. (2018). *Fourth national climate assessment*. https://nca2018.globalchange.gov/downloads/NCA4_Ch00_Front-Matter.pdf

Berghuijs, W. R., Woods, R. A., Hutton, C. J., & Sivapalan, M. (2016). Dominant flood generating mechanisms across the United States. *Geophysical Research Letters*, *43*(9), 4382–4390. https://doi.org/10.1002/2016gl068070

Breiman, L. (2001). Random Forests. *Machine Learning*, *45*(1), 5–32. https://doi.org/10.1023/A:1010933404324

Costabile, P., & Macchione, F. (2015). Enhancing river model set-up for 2-D dynamic flood modelling. *Environmental Modelling & Software*, *67*, 89–107. https://doi.org/10.1016/j.envsoft.2015.01.009

Coxon, G., Addor, N., Bloomfield, J. P., Freer, J., Fry, M., Hannaford, J., Howden, N. J. K., Lane, R., Lewis, M., Robinson, E. L., Wagener, T., & Woods, R. (2020). CAMELS-GB: hydrometeorological time series and landscape attributes for 671 catchments in Great Britain. In Earth System Science Data (Vol. 12, Issue 4, pp. 2459–2483). https://doi.org/10.5194/essd-12-2459-2020

Cui, Z., Chen, W., He, Y., & Chen, Y. (2015). Optimal Action Extraction for Random Forests and Boosted Trees. *Proceedings of the 21th ACM SIGKDD International Conference on Knowledge Discovery and Data Mining*, 179–188. https://doi.org/10.1145/2783258.2783281

Dahl, T. E. (2014). *Status and Trends of Prairie Wetlands in the United States 1997 to 2009*. U.S. Fish and Wildlife Service. https://play.google.com/store/books/details?id=n9pNuwEACAAJ

Davenport, F. V., Burke, M., & Diffenbaugh, N. S. (2021). Contribution of historical precipitation change to US flood damages. In *Proceedings of the National Academy of Sciences* (Vol. 118, Issue 4, p. e2017524118). https://doi.org/10.1073/pnas.2017524118

Dobur, J. C., & Center, Southeast River Forecast. (2006). *An Analysis of the Geographic Distribution of Flash Flood Events across the Southeastern United States*. NOAA/National Weather Service, Southeast River Forecast Center, Peachtree ….

https://www.weather.gov/media/serfc/seFlashFlood.pdf

Dougherty, E., & Rasmussen, K. L. (2019). Climatology of Flood-Producing Storms and Their Associated Rainfall Characteristics in the United States. *Monthly Weather Review*, *147*(11), 3861–3877. https://doi.org/10.1175/MWR-D-19-0020.1

Elshorbagy, A., Corzo, G., Srinivasulu, S., & Solomatine, D. P. (2010). Experimental investigation of the predictive capabilities of data driven modeling techniques in hydrology - Part 1: Concepts and methodology. *Hydrology and Earth System Sciences*, *14*(10), 1931–1941. https://doi.org/10.5194/hess-14-1931-2010

Friedman, J. H. (2001). Greedy Function Approximation: A Gradient Boosting Machine. *Annals of Statistics*, *29*(5), 1189–1232. http://www.jstor.org/stable/2699986

Ghojogh, B., & Crowley, M. (2019). The Theory Behind Overfitting, Cross Validation, Regularization, Bagging, and Boosting: Tutorial. In *arXiv [stat.ML]*. http://arxiv.org/abs/1905.12787

Gulakhmadov, A., Chen, X., Gulahmadov, N., Liu, T., Anjum, M. N., & Rizwan, M. (2020). Simulation of the Potential Impacts of Projected Climate Change on Streamflow in the Vakhsh River Basin in Central Asia under CMIP5 RCP Scenarios. *WATER*, *12*(5), 1426. https://doi.org/10.3390/w12051426

Hall, J., Arheimer, B., Borga, M., Brázdil, R., Claps, P., Kiss, A., Kjeldsen, T. R., Kriaučiūnienė, J., Kundzewicz, Z. W., Lang, M., Llasat, M. C., Macdonald, N., McIntyre, N., Mediero, L., Merz, B., Merz, R., Molnar, P., Montanari, A., Neuhold, C., … Blöschl, G. (2014). Understanding flood regime changes in Europe: a state-of-the-art assessment. In *Hydrology and Earth System Sciences* (Vol. 18, Issue 7, pp. 2735–2772). https://doi.org/10.5194/hess-18-2735-2014

Heggen, R. J. (2001). Normalized antecedent precipitation index. *Journal of Hydrologic Engineering*, *6*(5), 377–381. https://doi.org/10.1061/(asce)1084-0699(2001)6:5(377)

Hirschboeck, K. K. (n.d.). *Some Perspectives on Climate and Floods in the Southwestern US*. http://geochange.er.usgs.gov/sw/changes/natural/floods/

Hirschboeck, K. K. (1991). Hydrology of floods and droughts, climate and floods. *Water-Supply Paper-Geological Survey (US)*, *2375*, 67–88.

Ho, T. K. (1995). Random decision forests. *Proceedings of 3rd International Conference on Document Analysis and Recognition*, *1*, 278–282 vol.1. https://doi.org/10.1109/ICDAR.1995.598994

Hochreiter, S., & Schmidhuber, J. (1997). Long short-term memory. *Neural Computation*, *9*(8), 1735–1780. https://doi.org/10.1162/neco.1997.9.8.1735

Holm, S. (1979). A Simple Sequentially Rejective Multiple Test Procedure. *Scandinavian Journal* *of Statistics, Theory and Applications*, *6*(2), 65–70. http://www.jstor.org/stable/4615733

Hrachowitz, M., Savenije, H. H. G., Blöschl, G., McDonnell, J. J., Sivapalan, M., Pomeroy, J. W., Arheimer, B., Blume, T., Clark, M. P., Ehret, U., Fenicia, F., Freer, J. E., Gelfan, A., Gupta, H. V., Hughes, D. A., Hut, R. W., Montanari, A., Pande, S., Tetzlaff, D., … Cudennec, C. (2013). A decade of Predictions in Ungauged Basins (PUB)—a review. *Hydrological Sciences Journal*, *58*(6), 1198–1255. https://doi.org/10.1080/02626667.2013.803183

Hu, L., Nikolopoulos, E. I., Marra, F., & Anagnostou, E. N. (2020). Sensitivity of flood frequency analysis to data record, statistical model, and parameter estimation methods: An evaluation over the contiguous United States. *J. Flood Risk Manag.*, *13*(1). https://doi.org/10.1111/jfr3.12580

Ivancic, T. J., & Shaw, S. B. (2015). Examining why trends in very heavy precipitation should not be mistaken for trends in very high river discharge. *Climatic Change*, *133*(4), 681–693. https://doi.org/10.1007/s10584-015-1476-1

Ivanov, V. Y., Vivoni, E. R., Bras, R. L., & Entekhabi, D. (2004). Catchment hydrologic response with a fully distributed triangulated irregular network model. Water Resources Research, 40(11). https://doi.org/10.1029/2004wr003218

Jarosińska, E., & Pierzga, K. (2017). Estimating Flood Quantiles on the Basis of Multi-Event Rainfall Simulation. In T. Hromadka & P. Rao (Eds.), *Flood Risk Management*. IntechOpen. https://doi.org/10.5772/intechopen.68648

Kasiviswanathan, K. S., He, J., Sudheer, K. P., & Tay, J.-H. (2016). Potential application of wavelet neural network ensemble to forecast streamflow for flood management. *Journal of Hydrology*, *536*, 161–173. https://doi.org/10.1016/j.jhydrol.2016.02.044

Ke, G., Meng, Q., Finley, T., Wang, T., Chen, W., Ma, W., Ye, Q., & Liu, T.-Y. (2017). Lightgbm: A highly efficient gradient boosting decision tree. *Advances in Neural Information Processing Systems*, *30*, 3146–3154. https://www.academia.edu/download/59228936/LightGBM_f20190512-55031-xxtk42.pdf

Kim, H. I., & Kim, B. H. (2020). Flood Hazard Rating Prediction for Urban Areas Using Random Forest and LSTM. *KSCE Journal of Civil Engineering*, *24*(12), 3884–3896. https://doi.org/10.1007/s12205-020-0951-z

Kim, J., Johnson, L., Cifelli, R., Thorstensen, A., & Chandrasekar, V. (2019). Assessment of antecedent moisture condition on flood frequency: An experimental study in Napa River Basin, CA. *Journal of Hydrology: Regional Studies*, *26*, 100629. https://doi.org/10.1016/j.ejrh.2019.100629

Knight, S. K. (2010). From Flood Loss to FloodSmart: How FEMA's Mitigation Tools Work to Reduce the Impact of Flood Disasters. *38th Conference on Broadcast Meteorology*. https://ams.confex.com/ams/38Broadcast/techprogram/paper_169898.htm?pagewanted=all

Kohler, M. A., & Linsley, R. K. (1951). *Predicting the Runoff from Storm Rainfall*. U.S. Department of Commerce, Weather Bureau. https://play.google.com/store/books/details?id=XMtaTBhT5p4C

Kratzert, F., Klotz, D., Brenner, C., Schulz, K., & Herrnegger, M. (2018). Rainfall–runoff modelling using Long Short-Term Memory (LSTM) networks. *Hydrology and Earth System Sciences*, *22*(11), 6005–6022. https://doi.org/10.5194/hess-22-6005-2018

Kratzert, F., Klotz, D., Shalev, G., Klambauer, G., Hochreiter, S., & Nearing, G. (2019a). Benchmarking a catchment-Aware Long Short-Term Memory network (LSTM) for large-scale hydrological modeling. *Hydrology and Earth System Sciences Discussions*, 1–32. https://doi.org/10.5194/hess-2019-368

Kratzert, F., Klotz, D., Shalev, G., Klambauer, G., Hochreiter, S., & Nearing, G. (2019b). Towards learning universal, regional, and local hydrological behaviors via machine learning applied to large-sample datasets. *Hydrology and Earth System Sciences*, *23*(12), 5089–5110. https://doi.org/10.5194/hess-23-5089-2019

Kunkel, K. E., Stevens, L. E., Stevens, S. E., Sun, L., Janssen, E., Wuebbles, D., Kruk, M. C., Thomas, D., Shulski, M., Umphlett, N. A., Hubbard, K. G., Robbins, K., Romolo, L., Akyuz, A., Pathak, T. B., Bergantino, T. R., & Greg Dobson, J. (2013). *Regional Climate Trends and Scenarios for the U.S. National Climate Assessment Part 4. Climate of the U.S. Great Plains*. https://digitalcommons.unl.edu/hprccpubs/39/

Lara, A., Garcia, X., Bucci, F., & Ribas, A. (2017). What do people think about the flood risk? An experience with the residents of Talcahuano city, Chile. *Natural Hazards*, *85*(3), 1557–1575. https://doi.org/10.1007/s11069-016-2644-y

Lin, P., Yang, Z.-L., Gochis, D. J., Yu, W., Maidment, D. R., Somos-Valenzuela, M. A., & David, C. H. (2018). Implementation of a vector-based river network routing scheme in the community WRF-Hydro modeling framework for flood discharge simulation. Environmental Modelling & Software, 107, 1–11. https://doi.org/10.1016/j.envsoft.2018.05.018

Lins, H. F., & Slack, J. R. (2005). Seasonal and Regional Characteristics of U.S. Streamflow Trends in the United States from 1940 to 1999. *Physical Geography*, *26*(6), 489–501. https://doi.org/10.2747/0272-3646.26.6.489

Loh, W.-Y. (2002). REGRESSION TRESS WITH UNBIASED VARIABLE SELECTION AND INTERACTION DETECTION. *Statistica Sinica*, *12*(2), 361–386. http://www.jstor.org/stable/24306967

Mallakpour, I., & Villarini, G. (2015). The changing nature of flooding across the central United States. *Nature Climate Change*, *5*(3), 250–254. https://doi.org/10.1038/nclimate2516

Merz, B., Vorogushyn, S., Uhlemann, S., Delgado, J., & Hundecha, Y. (2012). HESS Opinions "More efforts and scientific rigour are needed to attribute trends in flood time series." *Hydrology* *and Earth System Sciences*, *16*(5), 1379–1387. https://doi.org/10.5194/hess-16-1379-2012

Milly, P. C. D., Wetherald, R. T., Dunne, K. A., & Delworth, T. L. (2002). Increasing risk of great floods in a changing climate. *Nature*, *415*(6871), 514–517. https://doi.org/10.1038/415514a

Mirzaei, S., Vafakhah, M., Pradhan, B., & Alavi, S. J. (2021). Flood susceptibility assessment using extreme gradient boosting (EGB), Iran. *Earth Science Informatics*, *14*(1), 51–67. https://doi.org/10.1007/s12145-020-00530-0

Mosavi, A., Ozturk, P., & Chau, K.-W. (2018). Flood Prediction Using Machine Learning Models: Literature Review. *WATER*, *10*(11), 1536. https://doi.org/10.3390/w10111536

Naghibi, S. A., Hashemi, H., Berndtsson, R., & Lee, S. (2020). Application of extreme gradient boosting and parallel random forest algorithms for assessing groundwater spring potential using DEM-derived factors. *Journal of Hydrology*, *589*, 125197. https://doi.org/10.1016/j.jhydrol.2020.125197

National Research Council, Division on Earth and Life Studies, Water Science and Technology Board, & Committee on the Scientific Bases of Colorado River Basin Water Management. (2007). *Colorado River Basin Water Management: Evaluating and Adjusting to Hydroclimatic Variability*. National Academies Press. https://play.google.com/store/books/details?id=n79VAgAAQBAJ

Naz, B. S., Kao, S.-C., Ashfaq, M., Rastogi, D., Mei, R., & Bowling, L. C. (2016). Regional hydrologic response to climate change in the conterminous United States using high-resolution hydroclimate simulations. *Global and Planetary Change*, *143*, 100–117. https://doi.org/10.1016/j.gloplacha.2016.06.003

Ncei, N. (2020). *NOAA National Centers for Environmental Information (NCEI) US billion-dollar weather and climate disasters*.

Newman, A. J., Clark, M. P., Sampson, K., Wood, A., Hay, L. E., Bock, A., Viger, R. J., Blodgett, D., Brekke, L., Arnold, J. R., Hopson, T., & Duan, Q. (2015). Development of a large-sample watershed-scale hydrometeorological data set for the contiguous USA: data set characteristics and assessment of regional variability in hydrologic model performance. *Hydrology and Earth System Sciences*, *19*(1), 209–223. https://doi.org/10.5194/hess-19-209-2015

Ni, L., Wang, D., Wu, J., Wang, Y., Tao, Y., Zhang, J., & Liu, J. (2020). Streamflow forecasting using extreme gradient boosting model coupled with Gaussian mixture model. *Journal of Hydrology*, *586*, 124901. https://doi.org/10.1016/j.jhydrol.2020.124901

Nikolopoulos, E. I., Anagnostou, E. N., Borga, M., Vivoni, E. R., & Papadopoulos, A. (2011). Sensitivity of a mountain basin flash flood to initial wetness condition and rainfall variability. *Journal of Hydrology*, *402*(3), 165–178. https://doi.org/10.1016/j.jhydrol.2010.12.020

Ouyang, Y., Zhang, J., Feng, G., Wan, Y., & Leininger, T. D. (2020). A century of precipitation trends in forest lands of the Lower Mississippi River Alluvial Valley. *Scientific Reports*, *10*(1), 12802. https://doi.org/10.1038/s41598-020-69508-8

Pan, Z., Arritt, R. W., Takle, E. S., Gutowski, W. J., Jr, Anderson, C. J., & Segal, M. (2004). Altered hydrologic feedback in a warming climate introduces a “warming hole.” *Geophysical Research Letters*, *31*(17). https://doi.org/10.1029/2004gl020528

Pathiraja, S., Westra, S., & Sharma, A. (2012). Why continuous simulation? The role of antecedent moisture in design flood estimation: THE ROLE OF ANTECEDENT MOISTURE IN DESIGN FLOOD ESTIMATION. *Water Resources Research*, *48*(6). https://doi.org/10.1029/2011wr010997

Pedregosa, F., Varoquaux, G., Gramfort, A., Michel, V., Thirion, B., Grisel, O., Blondel, M., Prettenhofer, P., Weiss, R., Dubourg, V., & Others. (2011). Scikit-learn: Machine learning in Python. *The Journal of Machine Learning Research*, *12*, 2825–2830.

Perry, C. A. (2000). *Significant floods in the United States during the 20th century - USGS measures a century of floods*. US Geological Survey. https://doi.org/10.3133/fs02400

Prein, A. F., Rasmussen, R. M., Ikeda, K., Liu, C., Clark, M. P., & Holland, G. J. (2017). The future intensification of hourly precipitation extremes. *Nature Climate Change*, *7*(1), 48–52. https://doi.org/10.1038/nclimate3168

Pryor, S. C. (2013). *Climate Change in the Midwest: Impacts, Risks, Vulnerability, and Adaptation*. Indiana University Press. https://play.google.com/store/books/details?id=BkwwbhZh0mkC

Razavi Tara, & Coulibaly Paulin. (2013). Streamflow Prediction in Ungauged Basins: Review of Regionalization Methods. *Journal of Hydrologic Engineering*, *18*(8), 958–975. https://doi.org/10.1061/(ASCE)HE.1943-5584.0000690

Remesan, R., & Mathew, J. (2014). *Hydrological Data Driven Modelling: A Case Study Approach*. Springer. https://play.google.com/store/books/details?id=lessBQAAQBAJ

Saadi, M., Oudin, L., & Ribstein, P. (2020). Beyond imperviousness: The role of antecedent wetness in runoff generation in urbanized catchments. *Water Resources Research*, *56*(11). https://doi.org/10.1029/2020wr028060

Saghafian, B., Golian, S., & Ghasemi, A. (n.d.). *Flood frequency analysis based on simulated peak discharges*. https://doi.org/10.1007/s11069-013-0925-2

Sagi, O., & Rokach, L. (2018). Ensemble learning: A survey. *Wiley Interdisciplinary Reviews. Data Mining and Knowledge Discovery*, *8*(4), e1249. https://doi.org/10.1002/widm.1249

Saharia, M., Kirstetter, P.-E., Vergara, H., Gourley, J. J., & Hong, Y. (2017). Characterization of floods in the United States. *Journal of Hydrology*, *548*, 524–535.

https://doi.org/10.1016/j.jhydrol.2017.03.010

Samaniego, L., Kumar, R., & Attinger, S. (2010). Multiscale parameter regionalization of a grid-based hydrologic model at the mesoscale. In *Water Resources Research* (Vol. 46, Issue 5). https://doi.org/10.1029/2008wr007327

Schoppa, L., Disse, M., & Bachmair, S. (2020). Evaluating the performance of random forest for large-scale flood discharge simulation. *Journal of Hydrology*, *590*, 125531. https://doi.org/10.1016/j.jhydrol.2020.125531

Seneviratne, S., Nicholls, N., Easterling, D., Goodess, C., Kanae, S., Kossin, J., Luo, Y., Marengo, J., McInnes, K., Rahimi, M., Reichstein, M., Sorteberg, A., Vera, C., Zhang, X., Alexander, L. V., Allen, S., Benito, G., Cavazos, T., Clague, J., … Zwiers, F. W. (2012). *Changes in climate extremes and their impacts on the natural physical environment*. Columbia University. https://doi.org/10.7916/D8-6NBT-S431

Sharma, A., Wasko, C., & Lettenmaier, D. P. (2018). If precipitation extremes are increasing, why aren't floods? *Water Resources Research*, *54*(11), 8545–8551. https://doi.org/10.1029/2018wr023749

Singh, V. P. (1988). *Hydrologic Systems: Watershed modeling*. Prentice Hall. https://play.google.com/store/books/details?id=QbUPAQAAIAAJ

Slater, L. J., & Villarini, G. (2017). Evaluating the Drivers of Seasonal Streamflow in the U.S. Midwest. *WATER*, *9*(9), 695. https://doi.org/10.3390/w9090695

Srivastava, N., Hinton, G., Krizhevsky, A., Sutskever, I., & Salakhutdinov, R. (2014). Dropout: a simple way to prevent neural networks from overfitting. *Journal of Machine Learning Research: JMLR*, *15*(1), 1929–1958. https://www.jmlr.org/papers/volume15/srivastava14a/srivastava14a.pdf?utm_campaign=buffer&utm_content=buffer79b43&utm_medium=social&utm_source=twitter.com

Sucik, M. T., & Marks, E. (2015). The status and recent trends of wetlands in the United States. *US Department of Agriculture*.

Taksande, A. A., & Mohod, P. S. (2015). Applications of data mining in weather forecasting using frequent pattern growth algorithm. *Int. J. Sci. Res*, *4*(6), 3048–3051. https://pdfs.semanticscholar.org/127d/cf3760f28ce2f4955dae3bd7d227083deb51.pdf

Teuling, A. J., de Badts, E. A. G., Jansen, F. A., Fuchs, R., Buitink, J., Hoek van Dijke, A. J., & Sterling, S. M. (2019). Climate change, reforestation/afforestation, and urbanization impacts on evapotranspiration and streamflow in Europe. *Hydrology and Earth System Sciences*, *23*(9), 3631–3652. https://doi.org/10.5194/hess-23-3631-2019

Thornton, P. E., Thornton, M. M., Mayer, B. W., Wilhelmi, N., Wei, Y., Devarakonda, R., & Cook, R. (2012). *Daymet: Daily surface weather on a 1 km grid for North America, 1980-2008*.

https://doi.org/10.3334/ORNLDAAC/1219

Todini, E. (2007). Hydrological catchment modelling: past, present and future. *Hydrology and Earth System Sciences*, *11*(1), 468–482. https://doi.org/10.5194/hess-11-468-2007

Tomer, M. D., & Schilling, K. E. (2009). A simple approach to distinguish land-use and climate-change effects on watershed hydrology. *Journal of Hydrology*, *376*(1), 24–33. https://doi.org/10.1016/j.jhydrol.2009.07.029

Vadeboncoeur, M. A., Green, M. B., Asbjornsen, H., Campbell, J. L., Adams, M. B., Boyer, E. W., Burns, D. A., Fernandez, I. J., Mitchell, M. J., & Shanley, J. B. (2018). Systematic variation in evapotranspiration trends and drivers across the Northeastern United States. *Hydrological Processes*, *32*(23), 3547–3560. https://doi.org/10.1002/hyp.13278

Verry, E. S., & Kolka, R. K. (2003). Importance of wetlands to streamflow generation. *In: Renard, Kenneth G.; et Al., Eds. 1st Interagency Conference on Research in the Watersheds; 2003 October 27-30; Benson, AZ.[City, State]: US Department of Agriculture, Agricultural Research Service: 126-132*. https://www.fs.usda.gov/treesearch/pubs/14144

Viessman, W., & Lewis, G. L. (1996). *Introduction to Hydrology*. HarperCollins. https://play.google.com/store/books/details?id=lNK2QgAACAAJ

Wasko, C., & Sharma, A. (2017). Global assessment of flood and storm extremes with increased temperatures. In *Scientific Reports* (Vol. 7, Issue 1). https://doi.org/10.1038/s41598-017-08481-1

Westra, S., Alexander, L. V., & Zwiers, F. W. (2013). Global Increasing Trends in Annual Maximum Daily Precipitation. *Journal of Climate*, *26*(11), 3904–3918. https://doi.org/10.1175/JCLI-D-12-00502.1

Wing, O. E. J., Bates, P. D., Smith, A. M., Sampson, C. C., Johnson, K. A., Fargione, J., & Morefield, P. (2018). Estimates of present and future flood risk in the conterminous United States. *Environmental Research Letters: ERL [Web Site]*, *13*(3), 034023. https://doi.org/10.1088/1748-9326/aaac65

Xiang, Z., Yan, J., & Demir, I. (2020). A rainfall-runoff model with LSTM-based sequence-to-sequence learning. Water Resources Research, 56(1). https://doi.org/10.1029/2019wr025326

Yu, P.-S., Yang, T.-C., Chen, S.-Y., Kuo, C.-M., & Tseng, H.-W. (2017). Comparison of random forests and support vector machine for real-time radar-derived rainfall forecasting. *Journal of Hydrology*, *552*, 92–104. https://doi.org/10.1016/j.jhydrol.2017.06.020

Zhao, G., Pang, B., Xu, Z., Yue, J., & Tu, T. (2018). Mapping flood susceptibility in mountainous areas on a national scale in China. *The Science of the Total Environment*, *615*, 1133–1142. https://doi.org/10.1016/j.scitotenv.2017.10.037

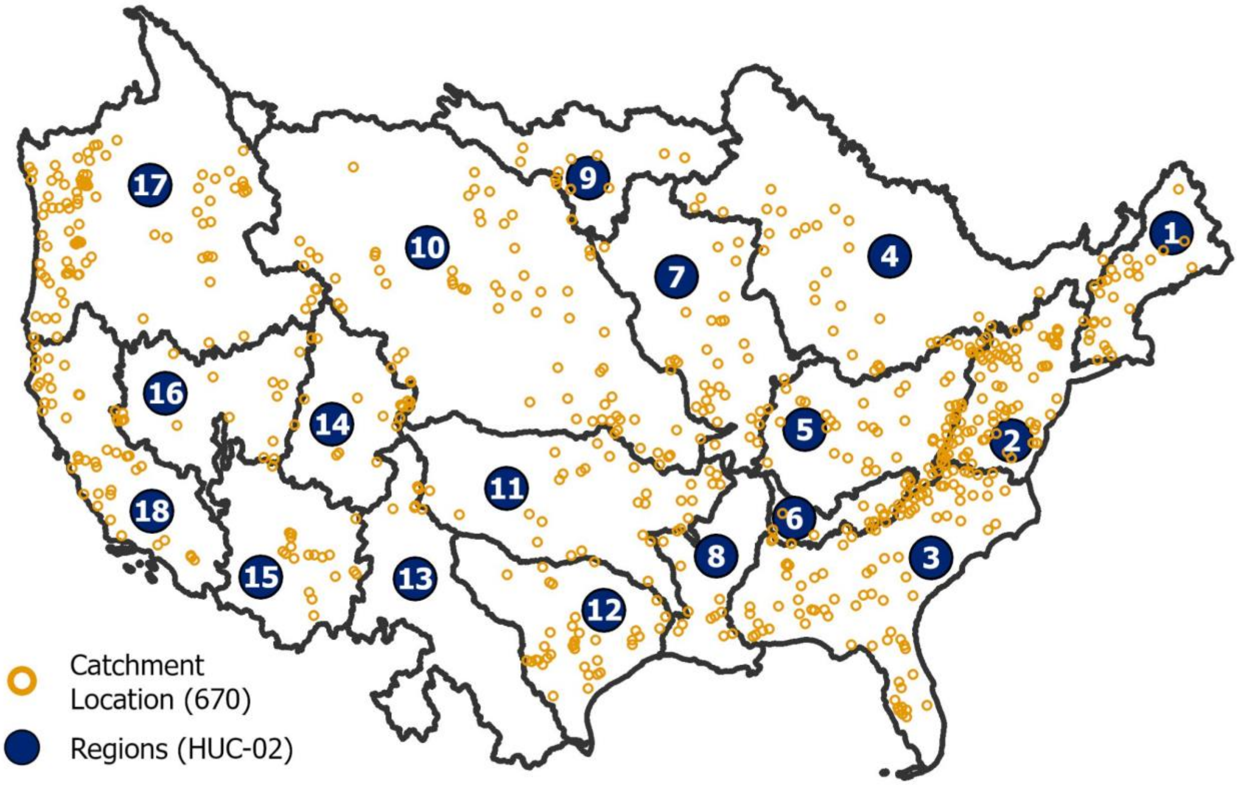

Figure 1: Location of the CAMELS' dataset's catchments across CONUS used in the study. Boundaries with numeric labels of the 18 hydroclimatic regions are also illustrated.

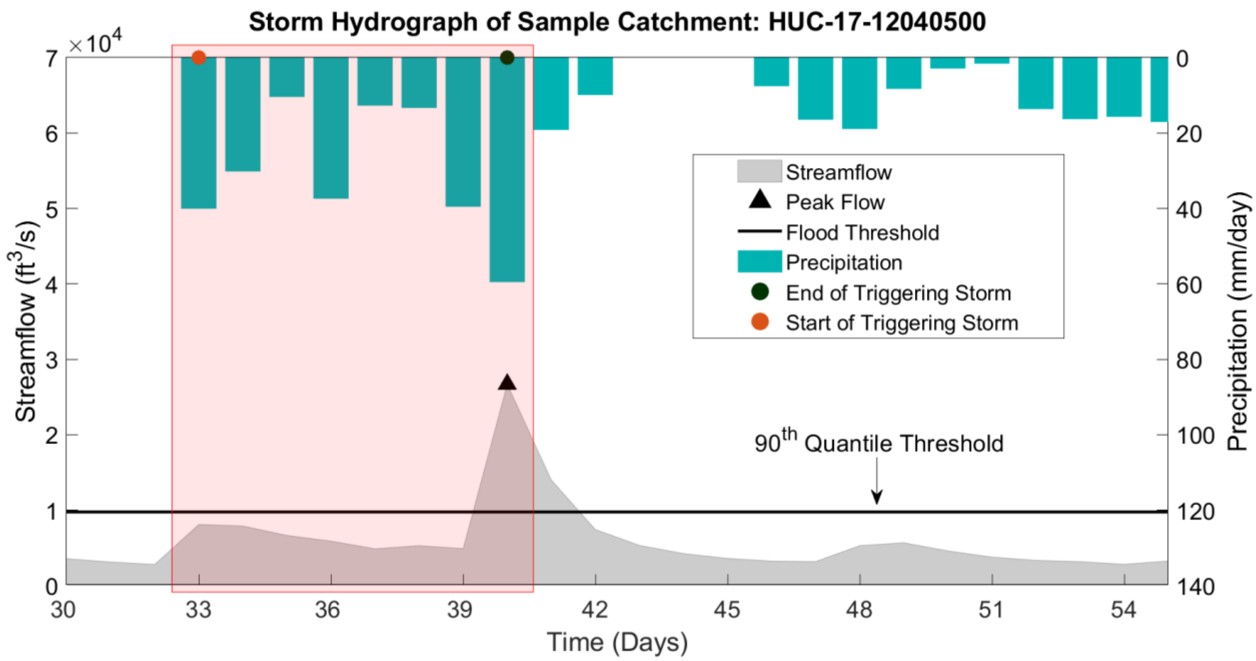

Figure 2: Sample illustration of preprocessing data in a catchment; the flows above the 90th streamflow quantile (grey patch at base) are isolated and considered peaks, then, the storm (blue bars) causing each peak is identified.

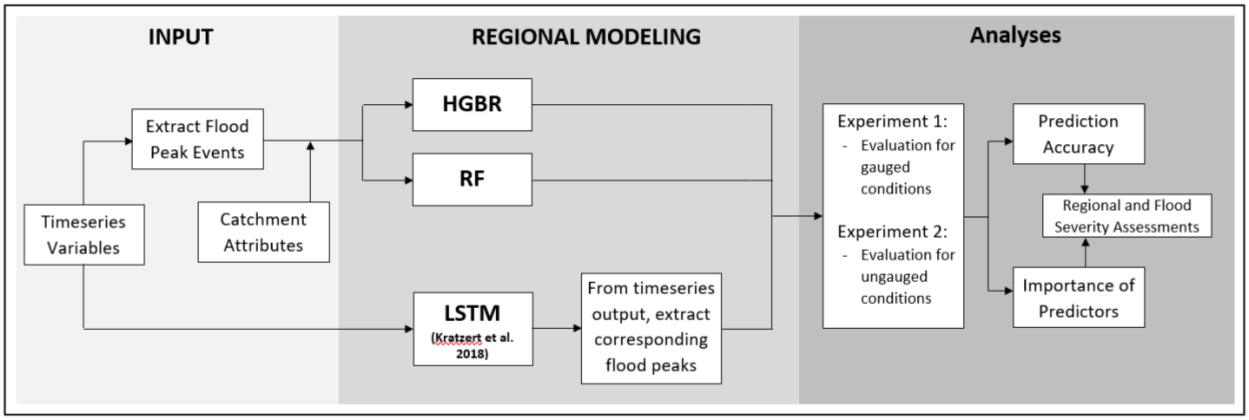

Figure 3: Methodology framework of the study. From streamflow and hydrometeorological time series, flood peak events were identified and together with static catchment attributes a flood peak database was built. Event-based inputs were used for the peak prediction models, HGBR and RF. The LSTM-based approach used time series inputs and the corresponding peak events extracted from the continuous streamflow output. Regional modeling of flood peaks was conducted under both gauged and ungauged catchment conditions, after which flood magnitude prediction and predictor importance were assessed.

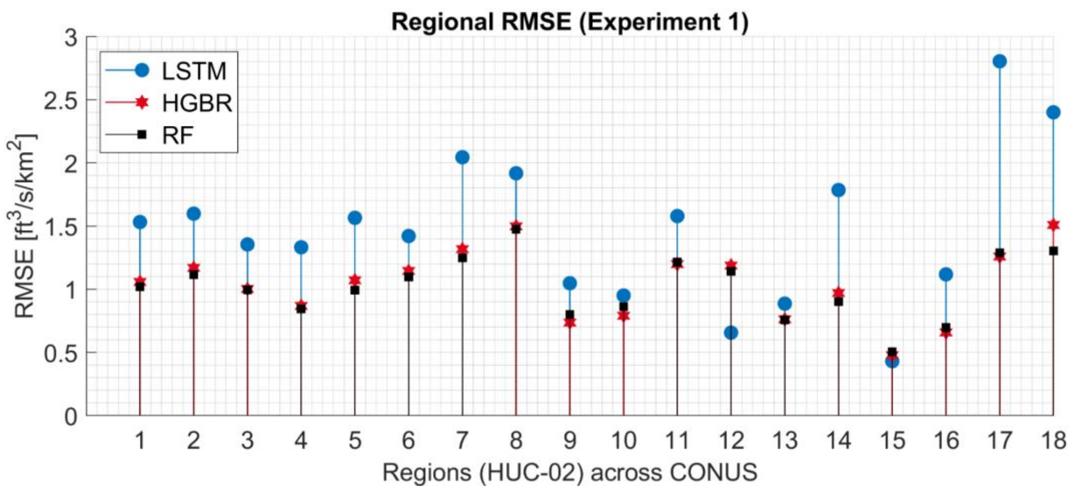

Figure 4: Experiment 1 (All Flows scenario) comparing the LSTM model with our two peak-predicting models (RF and HGBR). The stems represent median RMSE performance for the 18 regional models.

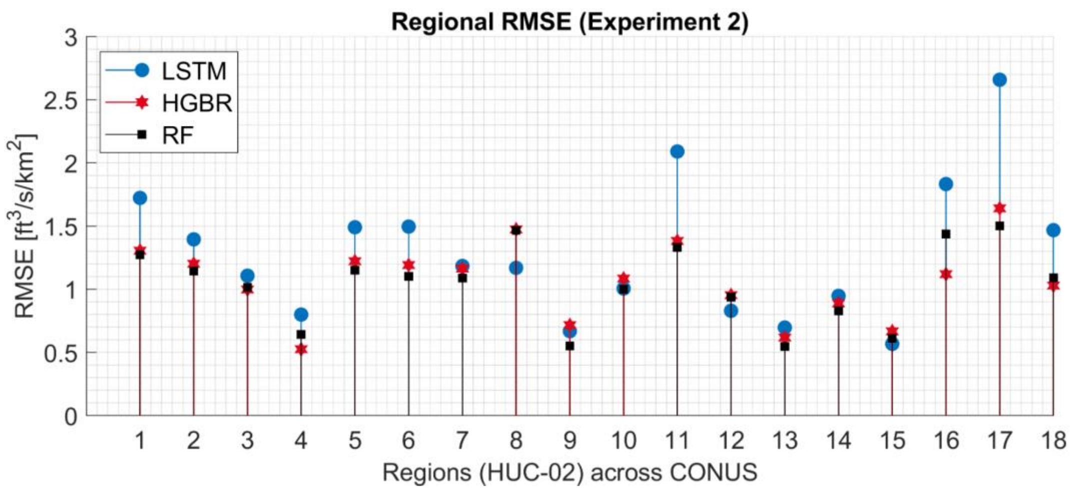

Figure 5: Same as described for Figure 4 but for Experiment 2

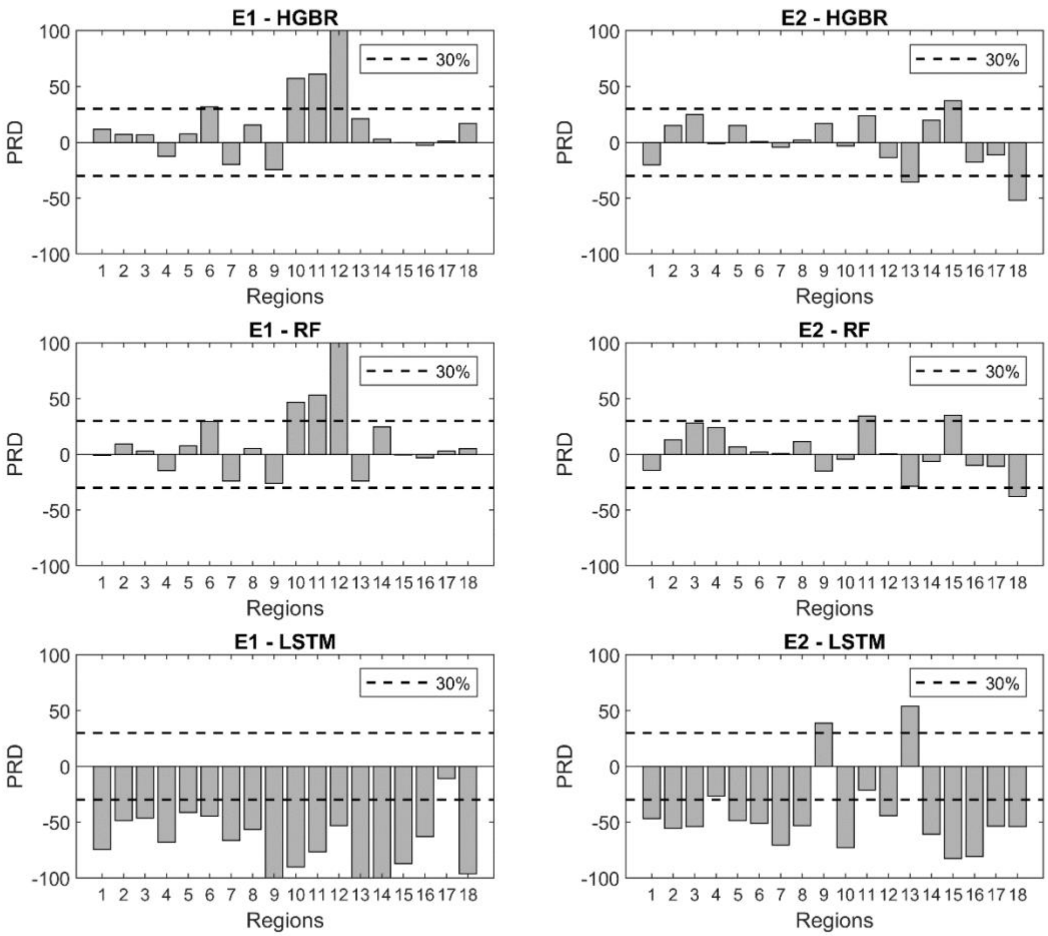

Figure 6: Percent Relative Difference (PRD) for the three models compared across the All-Flows scenario. PRD shown for both Experiments 1 (E1) and 2 (E2). The ±30% reference lines were the thresholds within which performance was considered acceptable. Interpretation of the PRD calculated indicates underestimation for bars below 0, whilst bars above 0 indicate overestimation.

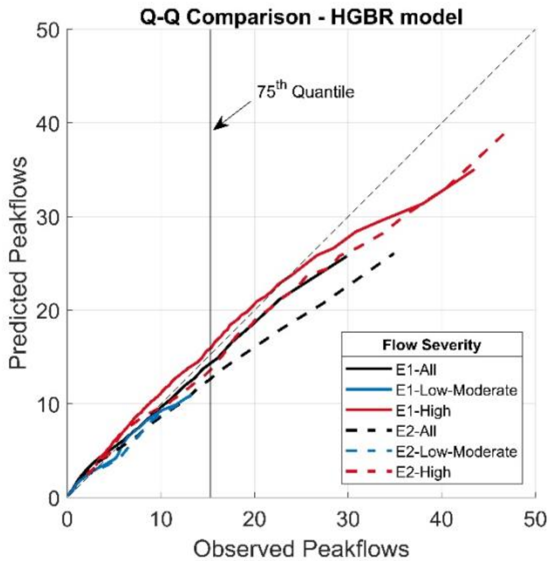

(a)

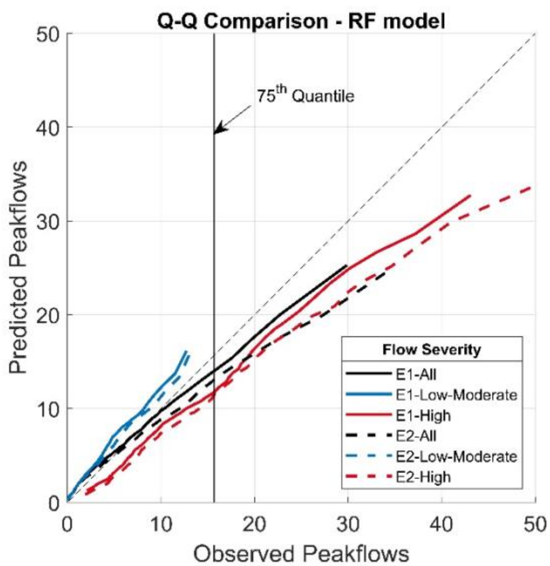

(b)

Figure 7: Quantile-Quantile comparison of the modeled output from the HGBR (a) and RF (b) models. Each plot compared the observed and predicted normalized peak flows for both Experiments 1 (E1) and 2 (E2) and for each flood severity scenario (All Flows; Low-Moderate Flows and High Flows). Vertical solid line is used to denote, for reference, the 75th quantile of observed peak flows.

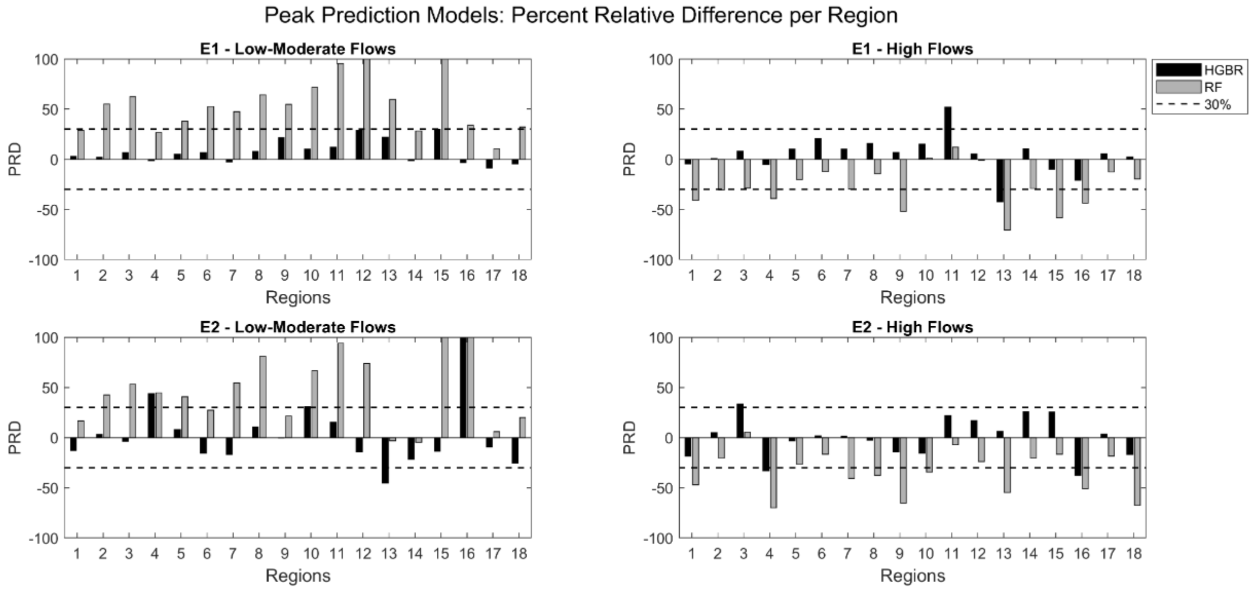

Figure 8: Percent Relative Difference (PRD) of the HGBR and RF models for both Experiments 1 (E1) and 2 (E2) and for all flood severities (Low-Moderate flows and High flows). The ±30% reference lines are the thresholds within which performance was considered acceptable. Interpretation of the PRD calculated indicates underestimation for bars below 0, whilst bars above 0 indicate overestimation.

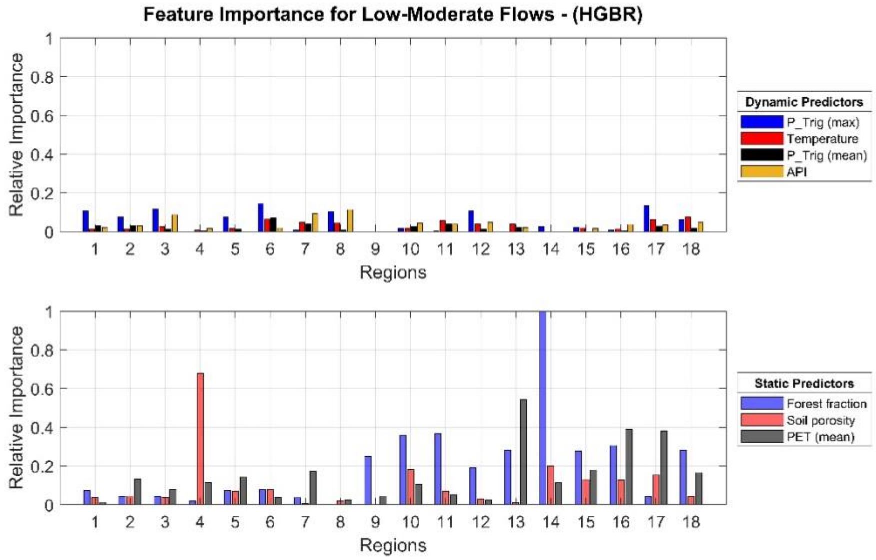

(a)

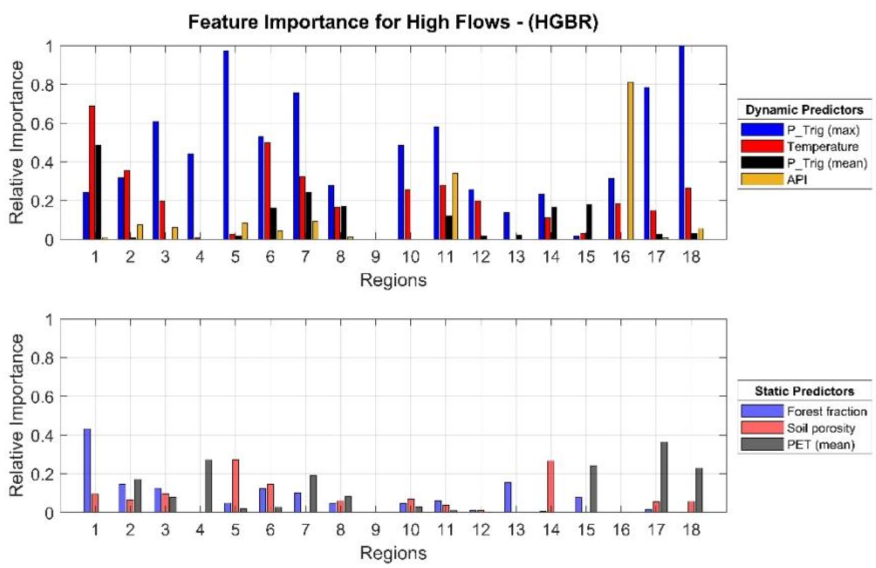

(b)

Figure 9: Relative Feature Importance distinguishing the flow severity levels: (a) Low-Moderate Flows (LMF) and (b) High Flows (HF). The dynamic variables are the maximum and mean triggering precipitation (P_Trig (max) and P_Trig (mean), respectively), the antecedent precipitation index (API) and temperature. The static catchment attributes are forest fraction, soil porosity and the mean potential evapotranspiration observed for the catchment (PET (mean)).

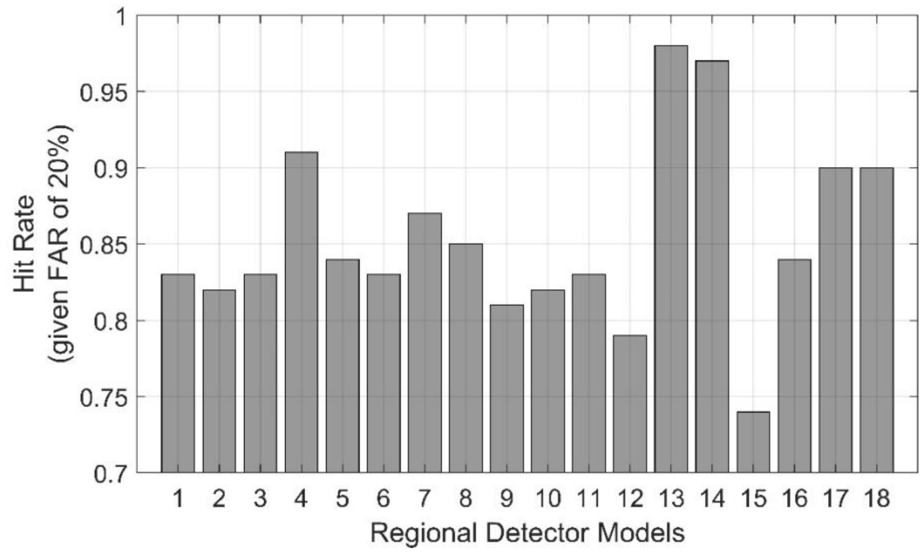

(a)

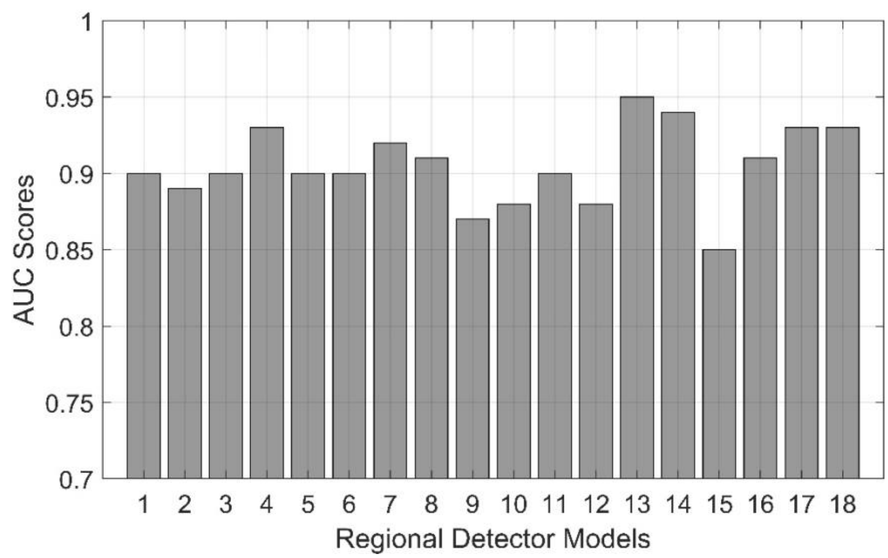

(b)

Figure 10: Hit rates for regional storm detectors corresponding to 20% false alarm rate from receiver operating characteristic (ROC) curves (a) and scores of the area under the ROC curves (AUC) are shown in (b).

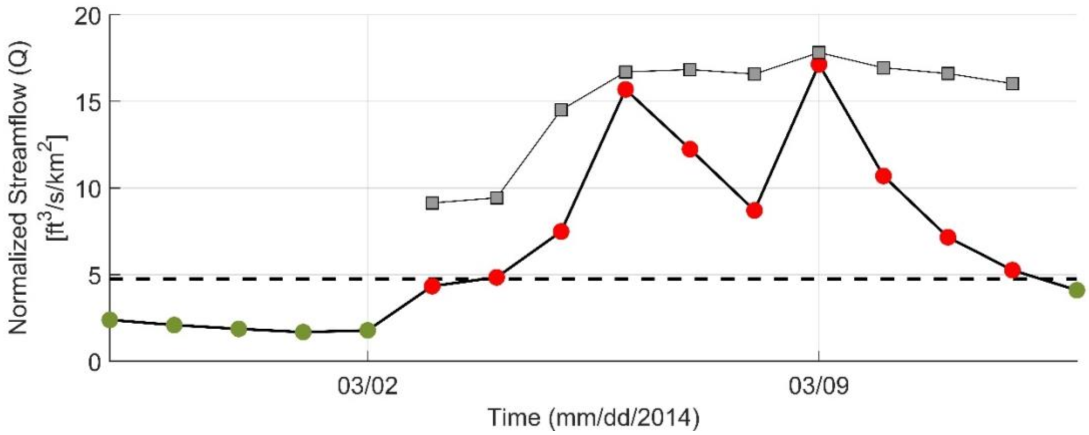

(a)

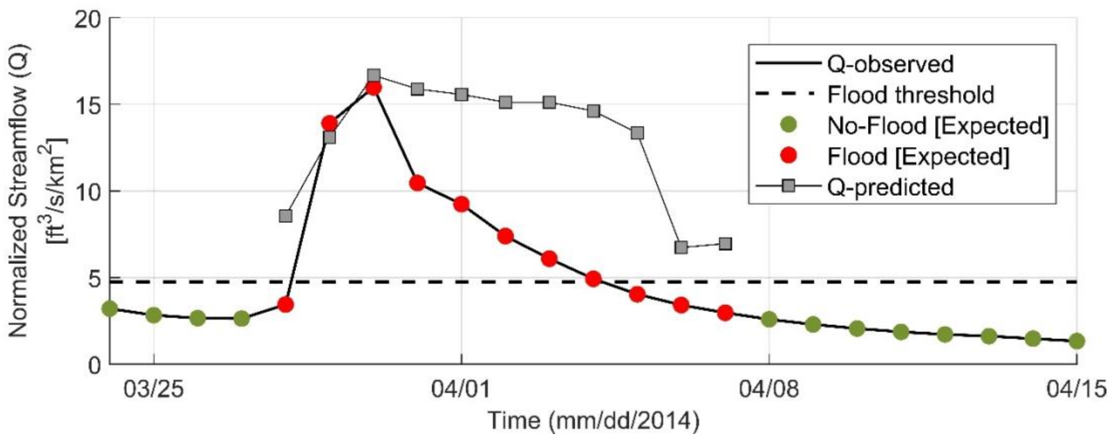

(b)

Figure 11: An illustration of the flood warning system for two extracted events (Fig. 11a: 03/02-13/2014; Fig. 11b: 03/24/2012 – 04/15/2012) monitored by gauge (ID: 12013500) located along the Willapa River near Willapa, Region 17. The figures provide the flood detector's response at each timestep along with predicted peak flow from the HGBR (All Flows model) if a flood event is expected.

Table 1: Distribution of catchments and events in the flood peak database generated for this study.

Region (HUC-02)		No. of Catchments	No. of Flood Peaks	Average No. of Flood Peaks per catchment
1	New England	27	3920	145
2	Mid-Atlantic	75	10990	147
3	South Atlantic Gulf	92	11395	124
4	Great Lakes	31	3324	107
5	Ohio	45	6783	151
6	Tennessee	17	2697	159
7	Upper Mississippi	33	3475	105
8	Lower Mississippi	12	1291	108
9	Soury-Red Rainy	9	300	33
10	Missouri	70	4376	63
11	Arkansas White-Red	31	2852	92
12	Texas Gulf	36	2516	70
13	Rio-Grande	7	209	30
14	Upper Colorado	17	467	27
15	Lower Colorado	19	1091	57
16	Great Basin	18	517	29
17	Pacific Northwest	91	8351	92
18	California	40	2451	61